Structural transformations in NiTi shape memory alloy nanowires

Reza Mirzaeifar,[1,a)] Ken Gall,[1,2] Ting Zhu,[1] Arash Yavari,[1,3] and Reginald DesRoches[3]
[1]George W. Woodruff School of Mechanical Engineering, Georgia Institute of Technology, Atlanta, Georgia 30332, USA
[2]School of Materials Science and Engineering, Georgia Institute of Technology, Atlanta, Georgia 30332, USA
[3]School of Civil and Environmental Engineering, Georgia Institute of Technology, Atlanta, Georgia 30332, USA

(Received 26 February 2014; accepted 3 May 2014; published online 20 May 2014)

Martensitic phase transformation in bulk Nickle-Titanium (NiTi)—the most widely used shape memory alloy—has been extensively studied in the past. However, the structures and properties of nanostructured NiTi remain poorly understood. Here, we perform molecular dynamics simulations to study structural transformations in NiTi nanowires. We find that the tendency to reduce the surface energy in NiTi nanowires can lead to a new phase transformation mechanism from the austenitic B2 to the martensitic B19 phase. We further show that the NiTi nanowires exhibit the pseudoelastic effects during thermo-mechanical cycling of loading and unloading via the B2 and B19 transformations. Our simulations also reveal the unique formation of compound twins, which are expected to dominate the patterning of the nanostructured NiTi alloys at high loads. This work provides the novel mechanistic insights into the martensitic phase transformations in nanostructured shape memory alloy systems. © *2014 AIP Publishing LLC*. [http://dx.doi.org/10.1063/1.4876715]

I. INTRODUCTION

The thermomechanical loading of NiTi alloys can cause the complicated structural transformations among various phases such as B2, B19, B19′, R, and base-centered orthorhombic (BCO), resulting in type-I, type-II, or compound twins.[1–3] While the martensitic phase transformation in bulk NiTi has been intensively studied, it still remains unclear how the surface affects phase transformation in nanostructured NiTi, despite some recent efforts.[4–9] The structure transformation and thermomechanical behavior of nanoscale materials can be remarkably different from their bulk counterparts.[10–13] Molecular dynamics simulations have shown the possibility of forming unexpected structures during temperature-driven phase transformation in equiatomic nanostructured NiTi.[6,7,14] We report here that the B19 martensite phase can be stable in NiTi nanowires due to a surface effect, although this phase was only reported stable in $Ni_{50}Ti_{50-x}Cu_x$ ($x \geq 7.5$) alloys in experiments.[15–17] The B19 martensite in bulk NiTi is meta-stable and tends to transform to the B19′ phase. However, our results show that cooling NiTi nanowires to temperatures below the martensite finish temperature, M_f, can induce a B2 → B19 transformation. The stability of the B19 phase is promoted by the tendency of free surfaces for reducing surface energy. The effect of free surfaces on making the B19 structure stable in nanowires is validated by studying the same temperature-driven phase transformation process in bulk NiTi with periodic boundary conditions. We show that in the absence of free surfaces, the B19 phase is unstable and transforms to B19′ or R-phase, consistent with early experimental and theoretical studies.[2,18–20]

II. METHODS

A many-body interatomic potential for the NiTi binary alloy is used in this work. The embedded atom potential (EAM) of NiTi was originally developed and evaluated by Lai and Liu.[21] This potential was improved by Zhong *et al.*[8] with a smooth cutoff behavior to avoid the diverging forces in simulations involving large atomic displacements. It was shown that the modified potential predicts the lattice constants and energies of the various phases of NiTi accurately compared to the *ab initio* calculations.[8,9] In order to study the temperature-driven structure transition in nanostructured NiTi, we start from a NiTi nanowire with its initial ordered B2 phase at $T = 500$ K, which is considerably higher than the austenite finish temperature, A_f, so as to enhance the stability of austenite. The nanowire is then cooled to the specified lower temperatures (250 K to 300 K) with a rate of 2 K per picosecond and equilibrated after cooling. Stress-driven phase transformation is also studied by applying an axial load to the nanowires. See supplementary material for the detailed methods of mechanical and thermal loadings on both bulk NiTi and nanowires.[22]

III. STABLE B19 PHASE

In our simulations, it is unexpectedly observed that the initial B2 structure in NiTi nanowires, favored at high temperatures, transforms to the B19 phase during cooling to low temperatures, while the B19′ structure is expected to be stable at low temperatures. Huang *et al.*[2] have studied the bulk NiTi single crystals using first-principles calculations based on density functional theory (DFT) and showed that the energy of B19 phase at zero K is lower than B2 and the R phase. However, since the B19 phase in NiTi is not typically observed in experiments at room temperature, they have proposed that B19 is mechanically unstable against a monoclinic distortion to the B19′ structure (or BCO, which is shown also

a)Present address: Laboratory for Atomistic and Molecular Mechanics, School of Civil and Environmental Engineering, Massachusetts Institute of Technology, Cambridge, Massachusetts 02139, USA. Electronic mail: rmirzaei@mit.edu

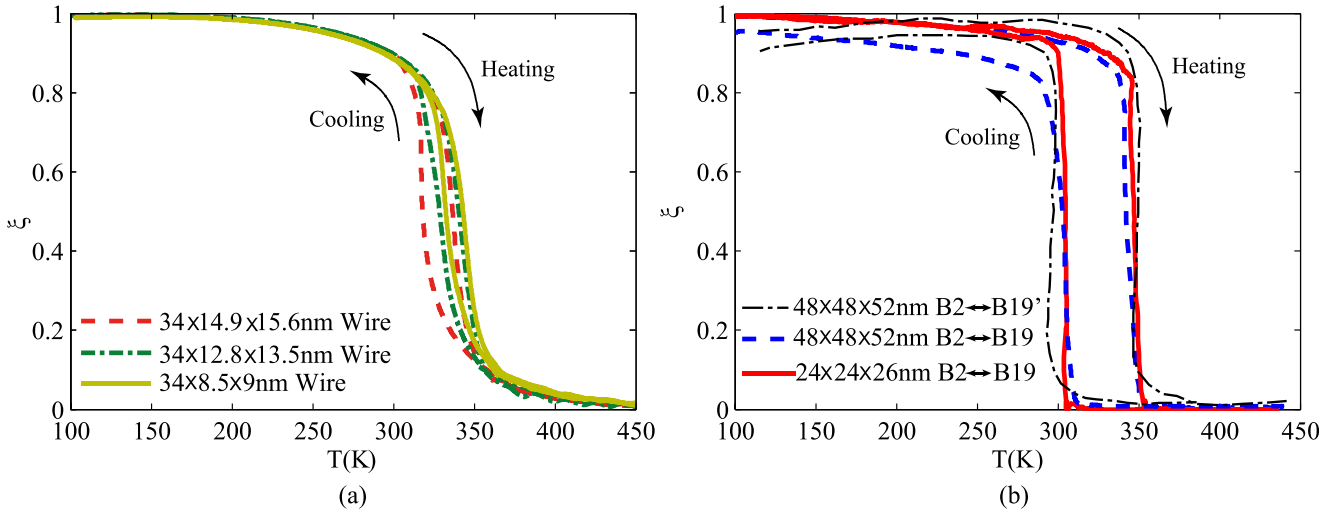

FIG. 1. MD simulation of temperature induced B2 ↔ B19 phase transformation for (a) nanowires with different sizes and (b) periodic supercells (the B2 ↔ B19′ phase transformation in bulk material is also shown in this figure). The order parameter ξ changes between 1 for B19 and B19′ structures and 0 for B2 structure.

to be stable in their work) due to a negative elastic modulus. However, our results show that in NiTi nanowires, the tendency of free surfaces to minimize their energy stabilizes the B19 phase. A similar phenomenon is recently reported for NiTi thin films based on Monte Carlo simulations.[14] Also, stable B19 phase has been observed in NiTiCu alloys with specific compositions.[15–17] This surface-driven phenomenon for NiTi systems is further studied next.

In the first step, we determine the transformation temperatures for the B2 ↔ B19 phase transformation. The effect of free surfaces and size on the transformation temperatures is studied in Figure 1. To distinguish the B2 and B19 phases, an order parameter is defined based on the lattice constants in the MD system as explained in supplementary material[22] (the order parameter ξ is set to zero for the B2 phase, and the two different B19 variants are denoted by $\xi = +1$ and -1 for the variants 1 and 2 shown with blue and red colors in Figure 2(a), respectively). Four different sizes of nanowires are considered. It was observed that the B2 ↔ B19 transformation is dominant for all these sizes in a heating-cooling cycle. The order parameter ξ during the heating-cooling cycle for the NiTi nanowires is shown in Figure 1(a). It is worth noting that a self-accommodated martensite is not formed in the nanowires, and the order parameter in Figure 1 corresponds to the absolute value of the order parameter for the only formed B19 variant. It is clear that the transformation temperatures are slightly changed by the size, likely due to the influence of surface energies. The temperature-driven phase transformation at zero stress in bulk NiTi is also studied using supercells with periodic boundary conditions. In this case, we considered the initial system with B19 structure equilibrated at 100 K (a crystallographic theory of phase transformation is used to construct the initial B19 structure by calculating the position of the atoms[23]). The system is then heated to 450 K and followed

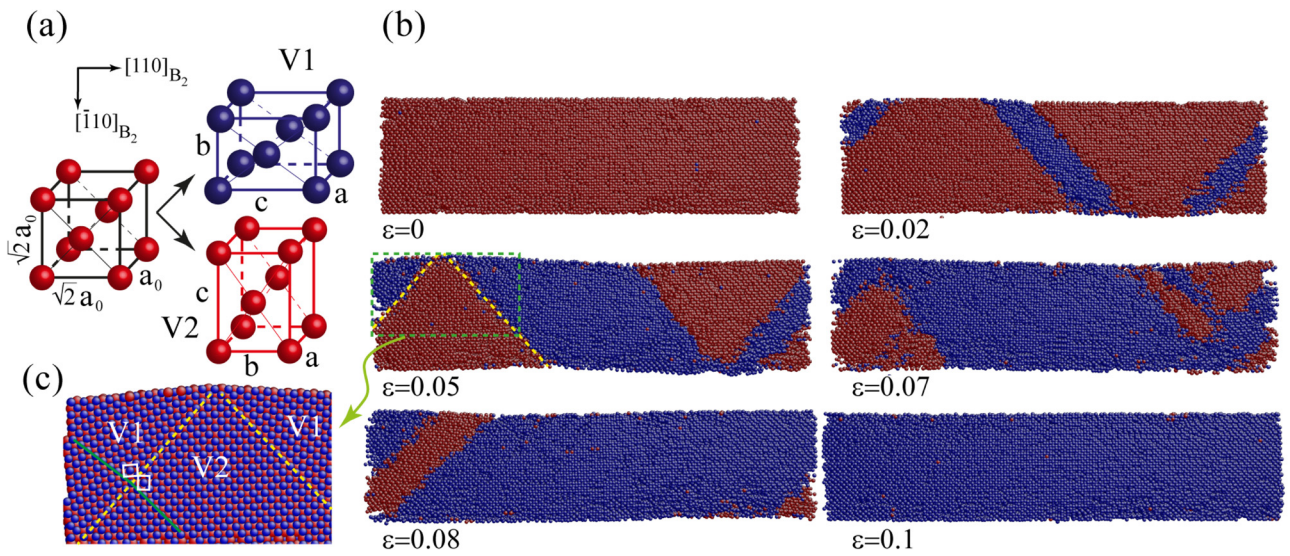

FIG. 2. Martensite reorientation in a 34 nm × 8.5 nm × 9 nm nanowire subjected to axial tensile load at T = 275 K. (a) Two different B19 variants and the B2 phase in $[110]_{B2}$ direction. (b) Reorientation patterns in the wire upon applying axial tension. Variants 1 and 2 (denoted respectively as V1 and V2) are shown with blue and red, respectively. (c) A closer view of multivariant interfaces in the nanowire. Ni an Ti atoms are shown with blue and red, respectively.

by cooling back to 100 K. During heating, a B19 → B2 phase transformation occurs. However, during cooling back to 100 K, a B2 → B19′ transformation happens in the periodic system, which is expected and previously reported.[8] Since we are interested in modeling the B2 ↔ B19 transformation, a geometric constraint is imposed on the system in which only the normal components of stress are relaxed. As a result, the forward and reverse B2 to B19 phase transformation in the system with periodic boundary conditions is achieved. The temperature-driven B2 ↔ B19 phase transformation in bulk NiTi is shown in Figure 1(b). Comparing Figures 1(a) and 1(b) clearly shows that while the size affects the transformation temperatures in nanowires slightly, it has a negligible effect with the periodic boundary conditions. For comparison, the B2 ↔ B19′ phase transformation in bulk NiTi with periodic boundary conditions is also shown in Figure 1(b). It is observed that the B2 to B19 and B19' transformation temperatures are almost identical for the bulk material.

IV. MARTENSITE REORIENTATION AND PHASE TRANSFORMATIONS

A. NiTi nanowires

Details of the structural transformations in NiTi nanowires are further studied by applying a tensile load on the system after the cooling stage. We focus on the stress driven structure transformations at temperatures below M_f. The nanowires are loaded in a strain controlled mode in the $[110]_{B2}$ direction at a constant strain rate of $1 \times 10^9\,s^{-1}$. In response to the tensile loading, the B19 phase, which is formed during the temperature-driven phase transformation in the cooling stage, reorients to a more favorable variant. This reorientation is associated with a pseudoelastic stress-strain response. The reorientation for a NiTi nanowire with dimensions 34 nm × 8.5 nm × 9 nm in x, y, and z directions subjected to an axial load at 275 K is presented in Figure 2.

As previously shown in Figure 1(a), B2 phase transforms to B19 during the cooling stage. The equilibrated structure at 275 K is B19 variant with the smaller lattice constant b along the axis of the wire as shown in Figure 2 at the axial strain of $\epsilon = 0$ (the atoms forming a variant 2 of B19 phase are shown with red color in this figure). It is observed that variant 2 reorients to variant 1 during the axial loading of the wire with a pattern shown in Figure 2. Formation of variant 1 initiates as three nanotwins in regions aligned in the equivalent $\sim \pm 45°$ directions with respect to the nanowire axis (see $\epsilon = 0.02$ in Figure 2). The reorientation propagates through the nanowire length during further axial straining. As observed in Figure 2 ($\epsilon = 0.07$), branching occurs inside the right twins and a new twin is formed inside the existing twins. The reorientation continues until the whole wire is transformed to variant 1 at the end of tensile loading ($\epsilon = 0.1$). The progressive reorientation leads to a pseudoelastic stress-strain response, to be further studied below. A similar study on a larger nanowire at two temperatures $T = 275$ and 300 K is also performed, and a similar reorientation pattern is observed (see supplementary material[22]). Figure 3 shows the stress-strain response for a NiTi nanowire subjected up to 10% axial strain and then unloaded to the initial length. The response is studied at three different temperatures: 250, 275, and 300 K.

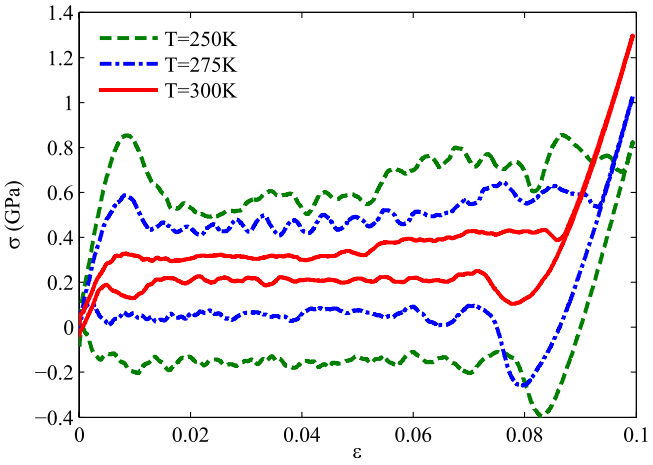

FIG. 3. The stress-strain curves corresponding to martensitic reorientation at three different temperatures for a 34 nm × 12.8 nm × 13.5 nm nanowire subjected to axial tensile loading-unloading.

Figure 3 reveals temperature effects on the stress-strain response of NiTi nanowires during reorientation. The main results are summarized as follows: (a) The slope of the initial elastic response of the nanowire is affected by the change of temperature. The initial linear response at the beginning of loading at all temperatures corresponds to the elastic deformation of variant 2 before the start of reorientation to variant 1. Interestingly, it is observed that this elastic response is temperature-dependent and the slope of the stress-strain curve decreases as the temperature increases. (b) The temperature affects the stress overshoot at the start of reorientation. As shown in Figure 3, the initiation of variant reorientation is associated with a stress overshoot at $T = 250$ K, while the stress-strain response is smooth at the initiation of reorientation at higher temperature $T = 300$ K. (c) The martensite reorientation completes at lower strains as the temperature increases. (d) The hysteresis area is reduced with increasing temperature. This phenomenon shows that the energy dissipation during martensite reorientation is decreased with increasing temperature. (e) The stress during reorientation is decreased by increasing the temperature. It is worth noting that the critical stress of phase transformation increases by increasing the temperature at high temperatures above A_f. However, our results in Figure 3 show that below M_f the reorientation critical stress decreases by increasing the temperature in NiTi nanowires. This phenomenon is consistent with the response of bulk NiTi as reported in experiments.[24,25]

B. Bulk NiTi

As mentioned earlier, our results show that the tendency of free surfaces to minimize their energy leads to the formation of stable B19 phase in NiTi nanowires. In order to further study the effect of free surfaces on the structure transformations, we also investigate similar temperature and stress-driven structure transformations in bulk NiTi using supercells with periodic boundary conditions. A representative study on

bulk NiTi is shown in Figure 4(b). It is observed that during cooling, the ordered B2 structure transforms to $\{100\}_{B2}\langle 011\rangle_{B2}$ twinned R-phase as shown in Figure 4 (see supplementary material for more details about forming the R-phase in bulk NiTi and the agreement of our results with experimental observations[22]). Similar to the nanowire case, the bulk NiTi is loaded to a 10% strain along the $[110]_{B2}$ direction after the cooling stage. The mechanical loading causes a R → B19′ transformation as shown in Figure 4(b). At the end of loading ($\epsilon = 0.1$), the B19′ martensite forms the self-accommodated compound $\{100\}_{B2}\langle 011\rangle_{B2}$ twins. This twinning system is consistent with both the theoretical calculations[26] and experimental observations[27–30] for equiatomic NiTi. Similar simulations are also performed at higher temperatures $T = 275$ K and 300 K. The corresponding phase transformation mechanism during cooling and mechanical loading is similar to that at $T = 250$ K (see supplementary material).[22] The stress-strain response associated with the R → B19' transformation is shown in Figure 4(a) for two different temperatures.

Comparison of Figures 2 and 4 clearly reveals the effect of free surfaces on the structure transformations in NiTi systems. This phenomenon raises the question regarding what constraints may promote formation of a stable B19 phase in the bulk material.

We have studied this condition by simulating periodic supercells in which only the normal stress components are relaxed at the boundaries during cooling the high temperature cubic B2 phase to lower temperatures. It is observed that this boundary condition causes a B2 → B19 transformation during cooling. However, despite the nanowire case in which the sidewalls are free surfaces and provide a preferred orientation for formation of one of the B19 variants, the equivalence of different directions in the periodic system leads to a self-accommodated B19 multivariant pattern as shown in the top row of Figure 5(a). This arrangement of two variants is extruded in the $[001]_{B2}$ direction as schematically shown in Figure 5(c). The system is then subjected to a displacement-controlled load in the $[110]_{B2}$ direction to a final strain of 10%. It is observed that variant 1 broadens while the variant 2 resolves during the mechanical loading. This phenomenon is expected since variant 1 is more favorable because the larger lattice constant is aligned along the straining direction in this variant. As shown, the whole system is reoriented to variant 1 at a strain $\epsilon = 0.05$, which is remarkably smaller compared to the value for nanowires. The stress-strain response for this case study is shown in Figure 5(b) at two different temperatures. The curves contain several parts with a negative slope during loading. These local peaks in the curves correspond to the propagation of martensite variant 1 in one of the twins, which is associated with resolving the other variant in the system. A similar example is also studied at T = 300 K (see supplementary material[22]). The broadening of variant 1 similarly occurs at T = 300 K. Comparing the results obtained for 300 K in Figure S4 (Ref. 22) with those obtained for 250 K in Figure 5 shows a refinement in martensite nanotwins at lower temperatures. This observation is in agreement with the Monte Carlo simulations of Zhong and Zhu[14] in NiTi thin films. The effect of size on the martensite patterns during B2 → B19 transformation is also studied by simulating larger supercells with periodic boundary conditions and relaxing only the normal pressure components during the cooling

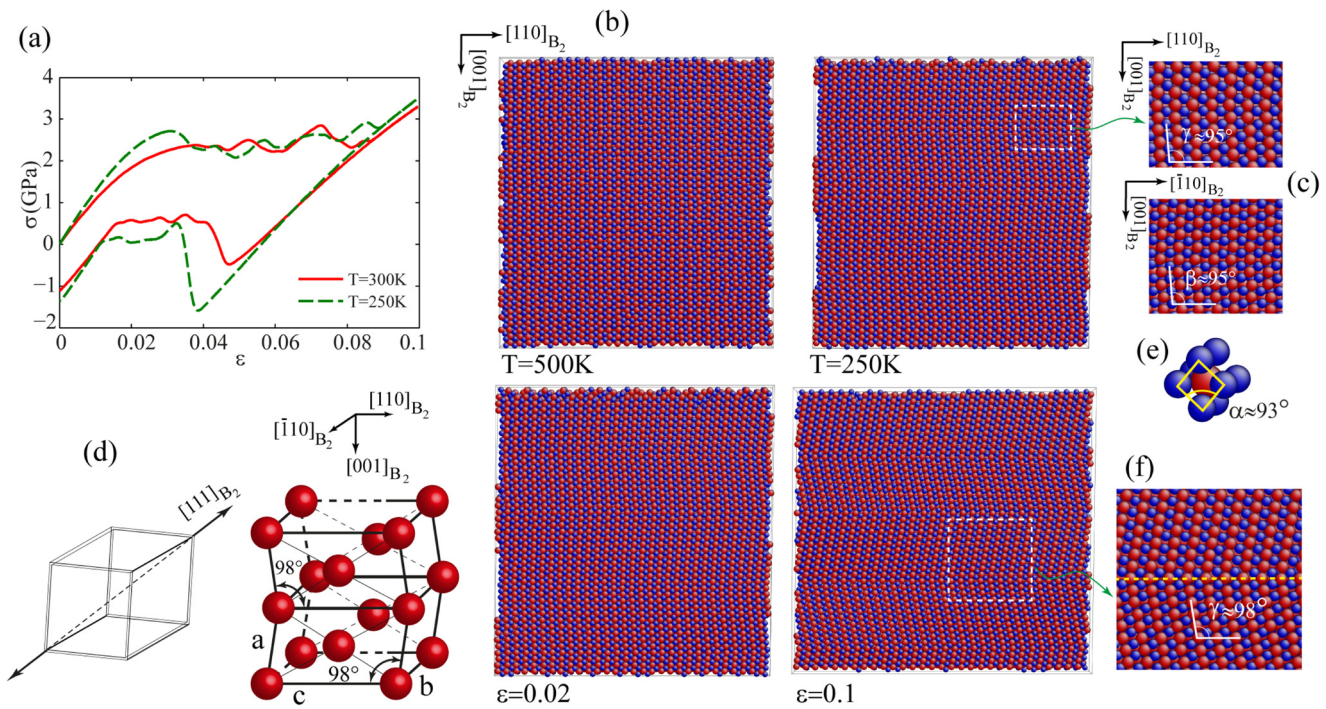

FIG. 4. A 12.8 nm × 12.8 nm × 13.5 nm supercell with periodic boundary conditions subjected to tensile loading. (a) The stress-strain response at two different temperatures. (b) $[\bar{1}10]$ view of the system during cooling and mechanical loading at 250 K. The supercell is cooled from initial B2 structure at 500 K to 250 K (first row), equilibrated at 250K, and then loaded in [110] direction (second row). (c) $[\bar{1}10]$ and [110] view of the R-phase at the end of cooling. (d) Schematic of the R-phase formed from elongation of the cubic cell in [111] direction and the B19′ twins. (e) Detected R-phase at the end of the cooling and measured α angle. (f) A close view of the B19′ compound twins at the end of mechanical loading.

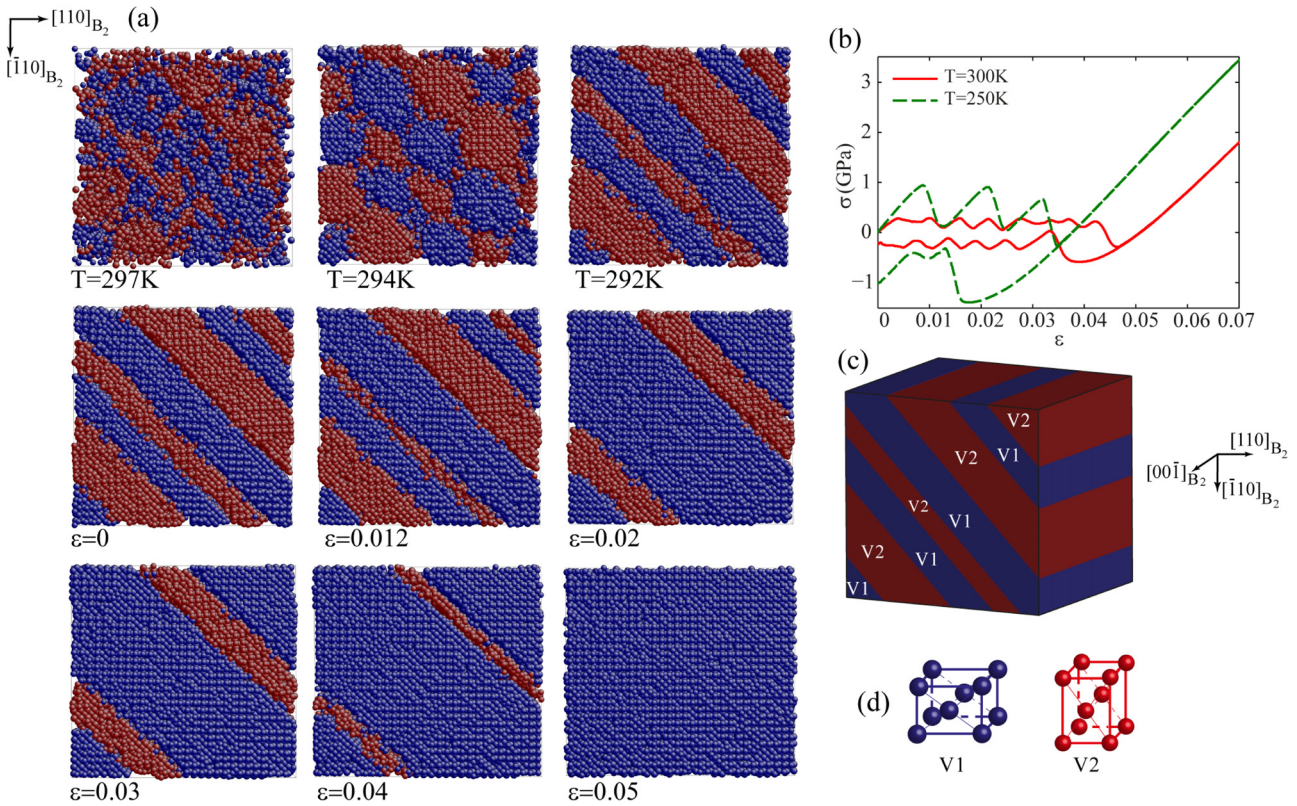

FIG. 5. A 12.8 nm × 12.8 nm × 13.5 nm supercell with special periodic boundary conditions (relaxing only the normal pressure components during cooling and equilibration stages) subjected to tensile loading. (a) [001] view of the system during cooling and mechanical loading at 250 K. The supercell is cooled from initial B2 structure at 500 K to 250 K (first row), equilibrated at 250K, and then loaded in [110] direction (second and third rows). (b) The stress-strain response at two different temperatures. (c) Schematic of the multivariant structure. (d) Schematic of the B19 variants. In this figure, blue and red colors represent variants 1 and 2, respectively.

stage. It is observed that the formation and propagation of multivariant martensite nanotwins is very similar in both sizes. This shows that the size effect is negligible in this study, and the results are representing a bulk material with an acceptable accuracy.[22]

V. NiTi NANOWIRES SUBJECTED TO ULTRA-HIGH TENSILE STRAINS

Finally, we study the structure transformation in NiTi nanowires subjected to ultra-high stresses. A tensile strain up to 20% is applied, after equilibrating the nanowire at temperatures below M_f. It was previously shown in Figure 2 that the nanowire is transformed to variant 1 of B19 phase at the end of axial loading to 10% strain. Further loading this single variant of B19 phase is associated with an elastic response (i.e., between II and III in Figure 6(b)). We observe that at a specific strain ($\epsilon \simeq 14\%$ for 300 K as marked with (III) in Figure 6(b)), the stress value decreases abruptly and the crystal structure changes by forming several self-accommodated nanotwins. Figure 6 shows the $[\bar{1}10]$ view of a 34 nm × 12.8 nm × 13.5 nm nanowire subjected to 20% axial strain at 300 K. It is observed at high strain levels (as shown for the strain values of 0.15 and 0.2) that several nanotwins are formed in the system. As shown in Figure 6(e) the crystal structure in the twins is BCO with a lattice tilt angle $\gamma \simeq 108°$. A schematic of the $\{100\}_{B2}\langle 011\rangle_{B2}$ BCO twins is also shown in this figure. This compound twinning system is reported in experimental observations for B19′ martensite[27–30] and also is proven to be energetically favorable based on studying generalized planar fault energy and generalized stacking fault energy barriers in NiTi.[26] Here, we show that the same type of compound twins is favorable in BCO structure when the NiTi system is subjected to ultra-high stresses.

Formation of these $\{100\}_{B2}\langle 011\rangle_{B2}$ nanotwins at ultra-high stresses can be explained by considering the Poisson effect. As the axial strain increases, the Poisson effect causes an increase in the lateral contraction in the nanowire. At a critical lateral contraction, the large negative lateral strain promotes strain accommodation by formation of multiple twins. This twinning system was previously reported for nanopillars subjected to an axial compression at lower strain levels ~5%,[9] which is consistent with our results since the negative lateral strain in tension is roughly one third of the axial strain. Another important observation during the B19 → BCO transformation is the mechanism of phase boundary propagation. As shown in Figures 6(b) and 6(c), the BCO twins propagate in a series of wedgelike regions toward the B19 phase. This phenomenon has been reported in experimental observations of interface between martensite and austenite in different shape memory alloys (SMAs).[23,24,31–33] A detailed view of the B19-BCO interface is shown in Figure 6.

In order to better understand the effect of size on the martensitic phase transformation in NiTi nanowires, we also

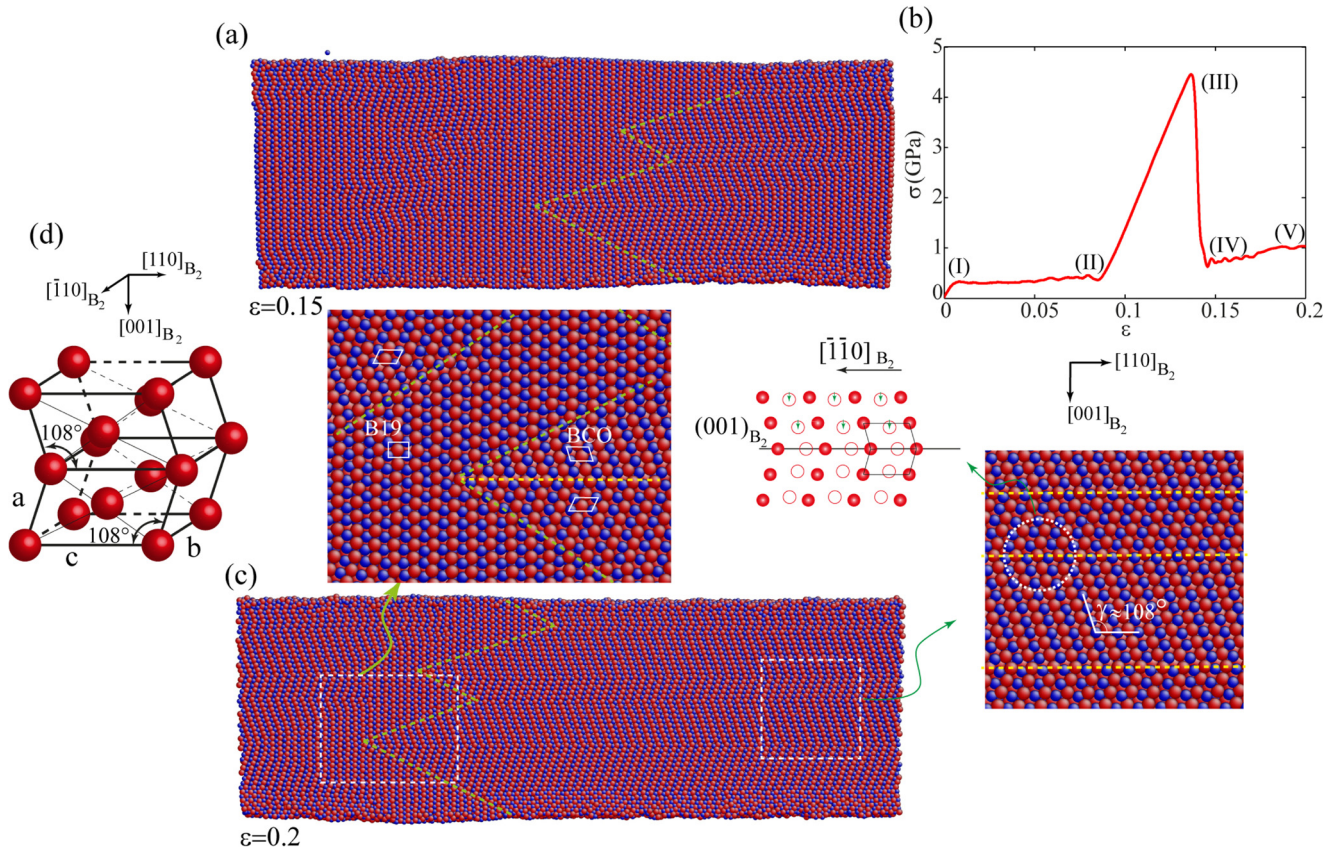

FIG. 6. Ultra-high stress response of a 34 nm × 12.8 nm × 13.5 nm nanowire subjected to 20% axial strain at 300 K. (a) and (c) $[\bar{1}10]$ view of the nanowire at two different strain values. The propagation of BCO twins into the B19 phase in wedgelike shapes is shown in the figures (BCO-B19 interfaces and the BCO twin planes are shown with dashed green and yellow lines, respectively). Ni an Ti atoms are shown with blue and red, respectively. (b) The stress-strain response of the wire. (d) Schematic of the BCO compound nanotwins (only Ti atoms are shown for clarity).

study the ultra-high stress response of NiTi nanowires with different sizes at different temperatures. The size effect on the solid-solid phase transformation has been studied for various alloys and geometries.[34–36] It was shown experimentally that free standing SMA nanowires of In-21 at. % Tl ranging in diameter from 650 to 10 nm do not show any size effect in the martensitic transformation as compared to the bulk material.[36] The ultra-high stress responses of NiTi nanowires with various sizes are studied as shown in Figure 7. The crystal structure of three different nanowires at 275 K

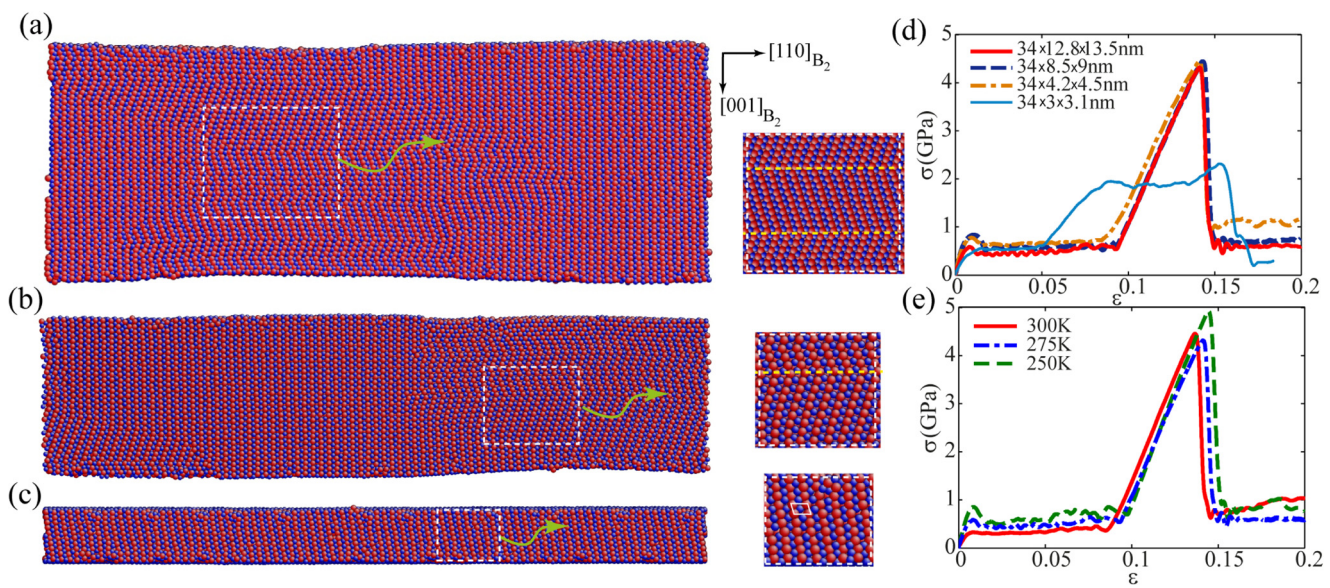

FIG. 7. The effect of size on the phase transformation and stress-strain response of NiTi nanowires. (a)–(c) $[\bar{1}10]$ view of three nanowires with different cross sections at 15% axial strain. Ni an Ti atoms are shown with blue and red, respectively. The effect of (d) size and (e) temperature on the stress-strain response of NiTi nanowires subjected to 20% axial strain.

subjected to a 15% axial strain is shown in Figures 7(a)–7(c). The length is identical for all the nanowires and the cross sections are (a) 12.8 nm × 13.5 nm, (b) 8.5 nm × 9 nm, and (c) 3 nm × 3.1 nm. Formation of several BCO twins in the largest wire is shown in Figure 7(a) similar to the previous case study at 300 K. A similar twinning pattern is also observed in the wire with smaller cross section 8.5 nm × 9 nm as shown in Figure 7(b). However, the phase transformation in very small wires is slightly different compared to the nanowires with larger cross sections. Figure 7(c) shows the crystal structure at 15% axial strain in a nanowire with 3 nm × 3.1 nm cross section. It is observed that during loading in contrast with the larger wires in which a reorientation occurs, in the very small nanowires variant 2 of B19 phase transforms to B19′ and then to BCO phase at higher strains ($\epsilon = 0.15$) as shown in Figure 7(c). More details of the phase transformation during cooling and also the crystal structure changes during mechanical loading for the small nanowire are given in supplementary material).[22] The transformation mechanism in this stage is also different from the larger wires in which self-accommodated nanotwins were formed in lateral direction (Figures 7(a) and 7(b)) and nanotwins are not formed in very small wires.

The stress-strain response of four nanowires with identical length and different cross sections is also shown in Figure 7(d). This figure shows that the formation of martensite lateral nanotwins in the wire is associated with an abrupt drop in the stress, which is consistent with the observed response in nanopillars subjected to an axial compression.[9] It is observed that the mechanical response is very similar for three sizes while the response of the smallest wire with a 3 nm × 3.1 nm cross section is different due to the difference in the transformation mechanisms as explained above. The temperature effect on the stress-strain response is shown in Figure 7(d) for nanowires with a 8.5 nm × 9 nm cross section. It is observed that the temperature slightly changes the critical stress corresponding to the start of the twinning.

VI. CONCLUSIONS

In this paper, we presented a comprehensive atomistic study of temperature- and stress-driven structure transformations in NiTi nanowires. Our MD simulations show that the tendency of free surfaces to minimize their energy in a nanowire leads to formation of a stable B19 phase. Our results show that the B19 phase at low temperatures reorients to a more favorable variant under a mechanical loading of the nanowire. The reorienting process is associated with a pseudoelastic stress-strain response at temperatures below the martensite finish temperature M_f. Our MD simulations also reveal the formation of $\{100\}_{B2}\langle 011\rangle_{B2}$ BCO compound twins in NiTi nanowires at ultra-high stresses, which propagate by growth of wedgelike regions into the parent B19 phase.

[1]M. Nishida, I. Itai, K. Kitamura, A. Chiba, and K. Yamauchi, "Effect of grain size of parent phase on twinning modes of B19′ martensite in an equiatomic Ti-Ni shape memory alloy," J. Phys. IV **5**(C8), 635 (1995).
[2]X. Y. Huang, G. J. Ackland, and K. M. Rabe, "Crystal structures and shape-memory behaviour of NiTi," Nature Mater. **2**, 307–311 (2003).
[3]K. Otsuka and X. Ren, "Physical metallurgy of Ti-Ni-based shape memory alloys," Prog. Mater. Sci. **50**, 511–678 (2005).
[4]T. Sato, K.-I. Saitoh, and N. Shinke, "Molecular dynamics study on microscopic mechanism for phase transformation of Ni-Ti alloy," Modell. Simul. Mater. Sci. Eng. **14**, S39–S46 (2006).
[5]K. Saitoh, T. Sato, and N. Shinke, "Atomic dynamics and energetics of martensitic transformation in nickel-titanium shape memory alloy," Mater. Trans. **47**, 742–749 (2006).
[6]D. Mutter and P. Nielaba, "Simulation of structural phase transitions in NiTi," Phys. Rev. B **82**, 224201 (2010).
[7]D. Mutter and P. Nielaba, "Simulation of the shape memory effect in a NiTi nano model system," J. Alloys Compd. **577S**, S83–S87 (2013).
[8]Y. Zhong, K. Gall, and T. Zhu, "Atomistic study of nanotwins in NiTi shape memory alloys," J. Appl. Phys. **110**, 033532 (2011).
[9]Y. Zhong, K. Gall, and T. Zhu, "Atomistic characterization of pseudoelasticity and shape memory in NiTi nanopillars," Acta Mater. **60**, 6301–6311 (2012).
[10]Y. Kondo, Q. Ru, and K. Takayanagi, "Thickness induced structural phase transition of gold nanofilm," Phys. Rev. Lett. **82**, 751–754 (1999).
[11]Y. Kondo and K. Takayanagi, "Synthesis and characterization of helical multi-shell gold nanowires," Science **289**, 606–608 (2000).
[12]A. Hasmy and E. Medina, "Thickness induced structural transition in suspended fcc metal nanofilms," Phys. Rev. Lett. **88**, 096103 (2002).
[13]J. K. Diao, K. Gall, and M. L. Dunn, "Surface-stress-induced phase transformation in metal nanowires," Nature Mater. **2**, 656–660 (2003).
[14]Y. Zhong and T. Zhu, "Patterning of martensitic nanotwins," Scr. Mater. **67**, 883–886 (2012).
[15]T. Saburi, Y. Watanabe, and S. Nenno, "Morphological characteristics of the orthorhombic martensite in a shape memory Ti-Ni-Cu alloy," ISIJ Int. **29**, 405–411 (1989).
[16]T. H. Nam, T. Saburi, Y. Nakata, and K. Shimizu, "Shape memory characteristics and lattice deformation in Ti-Ni-Cu alloys," Mater. Trans. JIM **31**, 1050–1056 (1990).
[17]P. Potapov, A. Shelyakov, and D. Schryvers, "On the crystal structure of TiNi-Cu martensite," Scr. Mater. **44**, 1–7 (2001).
[18]K. Parlinski and M. Parlinska-Wojtan, "Lattice dynamics of NiTi austenite, martensite, and R phase," Phys. Rev. B **66**, 064307 (2002).
[19]S. Kibey, H. Sehitoglu, and D. Johnson, "Energy landscape for martensitic phase transformation in shape memory NiTi," Acta Mater. **57**, 1624–1629 (2009).
[20]N. Hatcher, O. Y. Kontsevoi, and A. J. Freeman, "Role of elastic and shear stabilities in the martensitic transformation path of NiTi," Phys. Rev. B **80**, 144203 (2009).
[21]W. S. Lai and B. X. Liu, "Lattice stability of some Ni-Ti alloy phases versus their chemical composition and disordering," J. Phys.: Condens. Matter **12**, L53 (2000).
[22]See supplementary material at http://dx.doi.org/10.1063/1.4876715 for details of methods and more MD results.
[23]K. Bhattacharya, *Microstructure of Martensite: Why It Forms and How It Gives Rise to the Shape-Memory Effect* (Oxford University Press, 2003).
[24]K. Otsuka and C. M. Wayman, *Shape Memory Materials* (Cambridge University Press, 1999).
[25]K. Gall, H. Sehitoglu, Y. Chumlykov, I. Kireeva, and H. Maier, "The influence of aging on critical transformation stress levels and martensite start temperatures in NiTi: Part II-discussion of experimental results," Trans. ASME J. Eng. Mater. Technol. **121**, 28–37 (1999).
[26]T. Ezaz, H. Sehitoglu, and H. Maier, "Energetics of twinning in martensitic NiTi," Acta Mater. **59**, 5893–5904 (2011).
[27]T. Waitz, T. Antretter, F. Fischer, N. Simha, and H. Karnthaler, "Size effects on the martensitic phase transformation of NiTi nanograins," J. Mech. Phys. Solids **55**, 419–444 (2007).
[28]T. Waitz, D. Spišák, J. Hafner, and H. P. Karnthaler, "Size-dependent martensitic transformation path causing atomic-scale twinning of nanocrystalline NiTi shape memory alloys," EPL (Europhys. Lett.) **71**, 98–103 (2005).
[29]Y. Kudoh, M. Tokonami, S. Miyazaki, and K. Otsuka, "Crystal structure of the martensite in Ti-49.2 at. % Ni alloy analyzed by the single crystal X-ray diffraction method," Acta Metall. **33**, 2049–2056 (1985).
[30]M. Nishida, S. Ii, K. Kitamura, T. Furukawa, A. Chiba, T. Hara, and K. Hiraga, "New deformation twinning mode of B19′ martensite in Ti-Ni shape memory alloy," Scr. Mater. **39**, 1749–1754 (1998).

[31]K. Okamoto, S. Ichinose, K. Morii, K. Otsuka, and K. Shimizu, "Crystallography of β_1–γ_1 stress-induced martensitic transformation in a CuAlNi alloy," Acta Metall. **34**, 2065–2073 (1986).
[32]D. Liu and D. Dunne, "Atomic force microscope study of the interface of twinned martensite in copper-aluminium-nickel," Scr. Mater. **48**, 1611–1616 (2003).
[33]S. Stupkiewicz, G. Maciejewski, and H. Petryk, "Low-energy morphology of the interface layer between austenite and twinned martensite," Acta Mater. **55**, 6292–6306 (2007).
[34]Y. Chen and C. A. Schuh, "Size effects in shape memory alloy microwires," Acta Mater. **59**, 537–553 (2011).
[35]X. Wang, M. Rein, and J. J. Vlassak, "Crystallization kinetics of amorphous equiatomic NiTi thin films: Effect of film thickness," J. Appl. Phys. **103**, 023501 (2008).
[36]F. R. Phillips, D. Fang, H. Zheng, and D. C. Lagoudas, "Phase transformation in free-standing SMA nanowires," Acta Mater. **59**, 1871–1880 (2011).